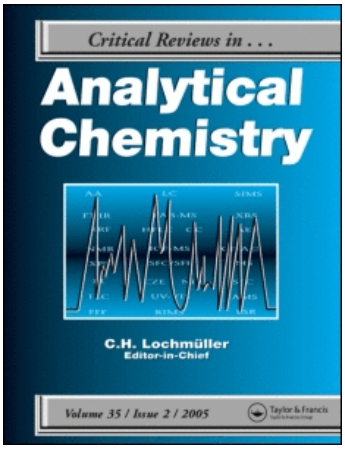

Critical Reviews in Analytical Chemistry
Publication details, including instructions for authors and subscription information:
http://www.informaworld.com/smpp/title~content=t713400837

Spectroscopic Applications of Laser-Induced Plasmas

Vahid Majidi[a]; Martha R. Joseph[a]
[a] Department of Chemistry, University of Kentucky, Lexington, Kentucky

To cite this Article Majidi, Vahid and Joseph, Martha R.(1992) 'Spectroscopic Applications of Laser-Induced Plasmas', Critical Reviews in Analytical Chemistry, 23: 3, 143 — 162
To link to this Article: DOI: 10.1080/10408349208050852
URL: http://dx.doi.org/10.1080/10408349208050852

Critical Reviews in Analytical Chemistry, 23(3):143–162 (1992)

Spectroscopic Applications of Laser-Induced Plasmas

Vahid Majidi and Martha R. Joseph*

Department of Chemistry, University of Kentucky, Lexington, Kentucky 40506

*Author to whom correspondence should be addressed.

ABSTRACT: Recent spectroscopic applications of laser-induced plasmas are reviewed. Virtually all substances are susceptible to breakdown when illuminated by a sufficiently intense laser beam. In a plasma, matter breaks apart into atoms, ions, and electrons, producing a visible flash and an audible popping sound due to the acoustical shock wave generated by the sudden, high-velocity expansion of matter outward from the plasma volume. Useful information about the elemental composition of the target material can be obtained from analysis of the emissions emanating from the plasma volume. Among the applications currently being tested in many laboratories are studies of particulate as well as gaseous pollutants in air, toxic substances present in flowing wastewater, elemental content of alloys, composition of iron ores and coal samples, contaminants on the surface of microcircuit boards, and the contents of fluid inclusions in geological samples. The beauty of laser-induced plasma spectroscopy is sample accessibility.

KEY WORDS: laser plasmas, analytical applications, atomic emission, microsampling, transient discharges.

I. INTRODUCTION

The purpose of this article is to review recent spectroscopic applications of the laser-induced plasma (LIP) and to acquaint the reader with some of the underlying principles. A comprehensive literature search on laser-produced plasmas (from 1987 to 1992) yielded more than 1000 citations; therefore, we have chosen to limit the scope of this review to cover publications regarding spectrochemical analysis since 1987. We are also providing some lead-in references for those readers who may be interested in other aspects of laser-generated plasmas. These include the interaction of magnetic and electric fields with LIP,[1-7] the influence of laser wavelength and pulse duration,[8,9] applications in mass spectrometry,[10-16] the effect of particles[17,18] and aerosols[8,19-23] on plasma production, time-resolved plasma imaging,[24-29] temperature and number density measurements,[30-34] ionization and plasma formation process,[35-40] UV and visible continuum light generation[41,42] and X-ray generation.[43-52]

A wealth of information is available on various aspects of the laser-generated plasma in earlier reviews and tutorial articles. Strasheim and Scott[53] presented a series of high-speed photographs that showed the plasma and crater formation when a pulsed high-energy laser beam was focused on metal targets. They also discussed the data collection system and provided spatially and temporally resolved emission spectra of several aluminum alloys. Potential applications in pollution monitoring and oil shale analysis by laser plasmas were introduced in a tutorial article by Loree et al.[54] In a review article by Adrian and Watson[55] on laser microspectral analysis, physical characteristics of laser plasmas were discussed in detail. In a more general review on weakly ionized plasmas by Blades and co-workers,[56] it was suggested that the optimal use of the laser plasma was for sampling process. Some selected applications of laser plasmas in analytical spectroscopy are provided in a comprehensive, application-oriented review on lasers in atomic spectroscopy by Thiem et al.[57] Recent experiments on the laser-induced breakdown of large transparent

1040-8347/92/$.50

liquid droplets were reviewed by Chang and co-workers.[58] Finally, the generation of homogeneous plasmas with prescribed density was discussed briefly by Bobin.[59]

One can find some reference to laser plasmas in practically any book written on the subject of high-intensity lasers. However, two of our favorite books specifically written on laser plasmas are *Laser-Induced Discharge Phenomena* by Raizer[60] and *Laser-Induced Plasmas and Applications,* which is a collection of chapters written by several authors and edited by Radziemski and Cremers.[61]

The authors would like to apologize in advance for any missed references and citations that should have been included in this review.

II. BACKGROUND

After the development of the Q-switched ruby laser, the next step toward forming an optically induced plasma only required placing a lens in the laser pathway to create the breakdown of air at the focal volume (first reported by Maker and co-workers[62]). The potential of this powerful tool for ablation, atomization, and ionization was obvious. Directing its power toward spectrochemical analysis, however, has been both a goal and a formidable challenge to spectroscopists. Laser-induced plasmas should be regarded as a universal sampling, excitation, and ionization source since optical plasmas can be formed in gases, liquids, and on solid substrates.[63] Furthermore, because the only requirement for the plasma formation is optical accessibility, these emission sources seem ideal for remote sensing. We should note that laser-induced plasma and laser-induced breakdown describe the same phenomena (i.e., generation of an optically ignited plasma). The laser breakdown terminology stems from the mechanism of plasma formation, which is similar in many ways to electrical breakdown. Nonetheless, some authors feel that laser-induced plasma is a more general term because electrical breakdown analogy falls short for plasmas generated in vacuum. A complete explanation of optical plasma generation due to various mechanisms can be found in books by Raizer[60] and Radziemski et al.[61] Figure 1 illustrates a general approach to the optical plasma formation. When a lens is used to concentrate a high-energy Q-switched laser pulse (>1 mJ) into a finite but small spot having a diameter of 2 ω_0, power densities in excess of GW/cm^2 will be attained at the focal volume. For example, the breakdown threshold (the minimum amount of optical energy needed to form a plasma) in air for a 7-ns laser pulse (at 532 nm) focused through a 12.7-mm focal length lens is 15.5 mJ. For the same system, a plasma can be formed in bulk water with as little as 5.4 mJ of optical energy. Currently, commercially available Nd:YAG lasers can generate up to 1 J of optical energy for a pulse duration of 5 ns, which is

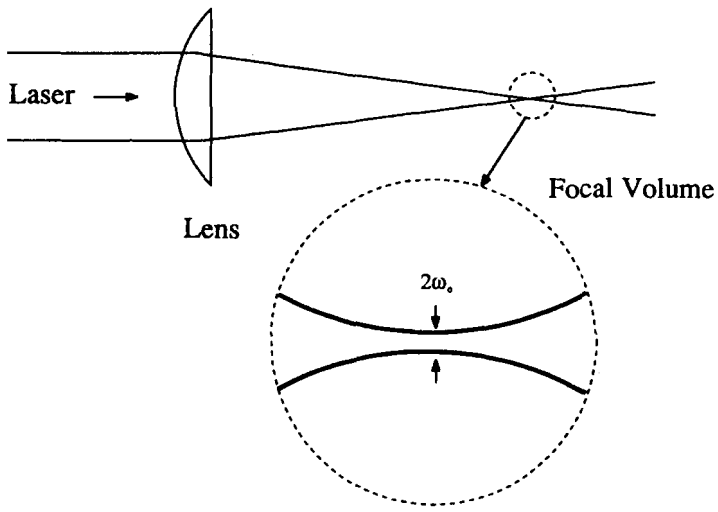

FIGURE 1. Typical optical geometry when a laser beam is focused Cross-section of the beam diameter is equal to 2 ω_0.

substantially higher peak power output than that required for most laser plasma experiments.

III. INSTRUMENTATION

A distinctive characteristic of laser-generated plasmas is their high temperatures. Radzimeski et al. [64] has shown that by focusing a 100-mJ pulse (15-ns duration) from a Q-switched laser, one can easily achieve power densities of GW/cm^2. They showed that the resulting plasma had an initial temperature of 25000 K and an electron number density of 10^{19} cm^{-3}. These temperatures and electron number densities are high enough to completely dissociate any matrix and generate a highly ionized plasma. Not surprisingly, these plasmas are well suited for atomic or ionic emission spectroscopy.

A typical instrumental setup for a laser plasma emission experiment is shown in Figure 2. The folding mirror is not essential for plasma formation; however, it is a convenient tool if lab space limitations are imposed on the experimenters. The laser and the focusing optics (i.e., the plasma-forming optics) should be considered as one component, because neither can generate a plasma individually. The requirement for the lens and the laser is simple: the laser/lens combination must be able to generate power densities in excess of 100 MW/cm^2 at the focal volume. As the laser output power is increased, one can form plasmas with progressively larger focal length lenses (yielding larger spot sizes). Conversely, if one has access to lasers with low output power, smaller focal length lenses must be utilized to form a plasma. In general, the least amount of power is required to form a plasma on solid substrates, liquids require more power, and gases are the most demanding.

The sample chamber can assume a variety of shapes and functions. In its simplest form it must provide a controlled atmosphere and optical access for the plasma to be formed, and it should provide a window for the data collection optics to view the plasma emission. In our laboratory, the sample chambers are made from Qwik flanges (also known as quick connect or NW type) assembled on 6-way crosses (37 mm tube diameter). This arrangement allows us to design various experiments on modular flanges that can be used for laser plasma spectrometry on solids, gases, and aerosols. Furthermore, various standard accessories can be purchased for optical access, electrical connections, and pressurizing or evacuating these chambers.

The emission from laser plasmas are typically collected orthogonal to the direction of the incoming laser beam to minimize possibility of damage to the detectors. A monochromator is used to separate

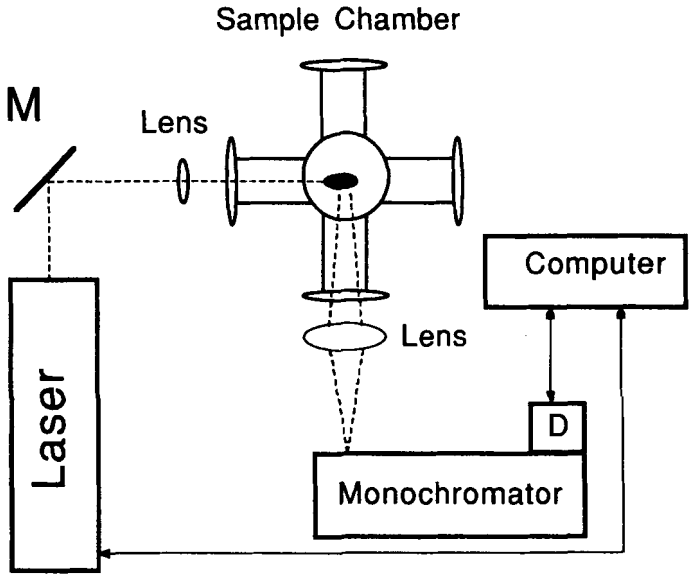

FIGURE 2. Instrumental arrangement for laser-induced plasma emission experiment. M, mirror; D, detector.

the plasma emission into its component wavelengths, which are then focused onto the detector. The photomultiplier (PMT) and photodiode array (PDA) are two of the most commonly used detectors for the emission measurements. In either case, it is desirable to have some type of gating capability for time-resolved data collection. The most attractive feature of the PDA is its ability to monitor several wavelengths simultaneously. PMTs, when combined with high-speed digitizers, can provide subnanosecond time resolution.

Although it is possible to collect temporally integrated data, due to the transient nature of the laser-induced plasmas, time-resolved data will provide optimum signal-to-noise and/or signal-to-background ratios. Therefore, if time resolution is sought, detection must be synchronized with the plasma generation. Many laboratories take advantage of the plasma luminosity itself and use it as the time marker. Utilization of this technique, however, limits observation of early events in the plasma due to inherent delays in electronics and in the plasma ignition process. Some of the results from the laser irradiation of a polyethylene target depicting spectral line intensities of various ionized states of carbon as a function of time are shown in Figure 3.[65] It is evident that plasma composition varies with position in the plasma volume, and with time elapsed. In some laboratories, including ours, a master oscillator and delay generator are used to keep track of timing sequence. In this type of setup, a computer is used to program the required events and timing sequence into a pulse/delay generator. The laser flashlamps are activated first, the Q-switch is then triggered, and the detection electronics are gated independently by the same pulse/delay generator to record a phenomena before, during, or after the plasma formation. The acquired information is typically transferred into the computer for data processing.

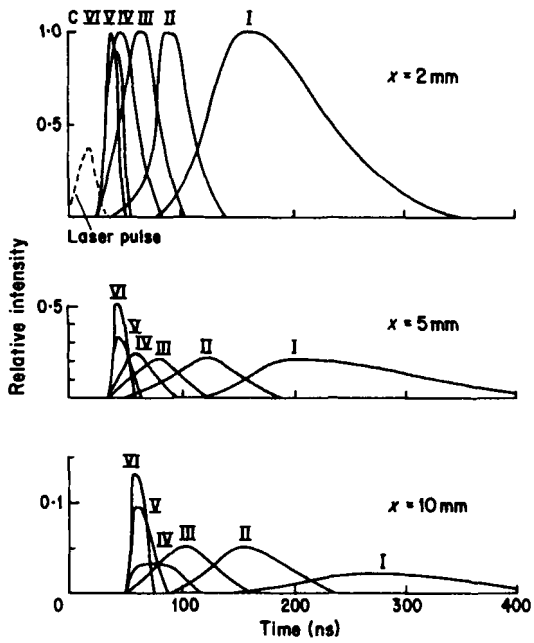

FIGURE 3. Carbon emissions resulting from a ruby laser irradiance of a polyethylene target. Time variation of lines of C(VI)-C(I), normalized to unity at the time of peak intensity at 2 mm from the surface. Distance from surface: A, 2 mm; B, 5 mm; C, 10 mm. (From Boland, B. C.; Irons, F. E.; McWhirter, R. W. P. *J. Phys. B (Proc. Phys. Soc.*, Ser. 2). 1968, *1*, **1180**. With permission.)

IV. RECENT APPLICATIONS

A. Single Phase Samples

Spectroscopic determinations are most frequently performed in gas-phase or in transparent liquid samples. However, a large number of publications on the determination of the composition of solid materials also exists. Applications for each of these phases are discussed individually.

1. Solids

The ability of LIP to vaporize micro quantities of a solid substance, thus making possible gas-phase analysis, has opened the door to a number of analytical applications. As in any new technique, known samples must be used to explore the qualitative and quantitative possibilities. Many research groups have LIP experimental results for standard samples, as well as applications to real situations.

Cremers[66] reported the results for remote multielemental analysis of metals. To evaluate the utility of laser plasmas as a remote sensing probe for elemental analysis, the fundamental beam from a Nd:YAG laser was focused to form a plasma on a metal surface up to 2.4 m away from the focusing optics. The resulting emissions were collected and transferred to a diode array rapid scanning spectrometer system by a quartz fiber optic. In these

experiments, eight metals were characterized over several 40-nm spectral regions to locate appropriate wavelengths suitable for multielemental detection. Figure 4 shows the composite emission spectrum for the 378.98- to 419.00-nm region. Using at least two spectral regions for each metal and ratioing the area under each peak against a background region, qualitative identification of targets containing Cu, Zn, Al, Ni, Sn, Mo, Ti, and Fe as the major constituent (>90%) was possible.

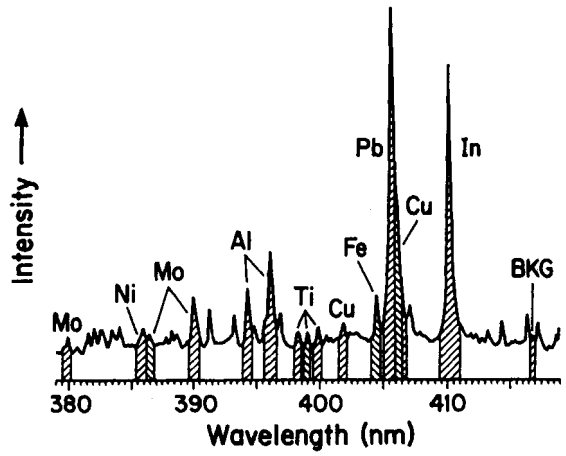

FIGURE 4. Composite spectrum of eight elements showing the lines and background region (BKG) used to identify different metals. (From Cremers, D. A. *Appl. Spectrosc.* 1987, *41*, **574**. With permission.)

Analysis of brass (Cu, Zn), Monel (Ni, Cu), as well as solders of varying Sn/Pb ratios were also performed.[66] Calibration curves were prepared from analysis of steel samples having known compositions. Testing these calibration curves to predict concentrations of known samples gave results with percent relative standard deviations (RSDs) ranging from 4 for Cr to 28 for Cu.

This technique was tested on metals whose surfaces were contaminated with oil, paint, and tape, and on the zinc coating on galvanized steel. Observation of the changes in the spectra as a single location on the sample was repeatedly hit by the laser spark provided information about both the surface contaminant and the bulk metal underneath it. Some contaminants were quickly removed, revealing the identity of the bulk metal; others were exceedingly resistant to ablation, especially the Zn coating of galvanized steel.

Quentmeier, Sdorra, and Niemax[67] determined the concentrations of Si, Cr, Mn and M in three metallic matrices (steel, copper, and aluminum). A Nd:YAG laser was used for the ablation of solid samples into a hot argon atmosphere, and then the resulting plasma was probed with an excimer pumped dye laser. The laser-induced fluorescence (LIF) radiation was detected by an optical multichannel analyzer (OMA) system. By comparing the fluorescence intensity ratios of the analytes to their respective concentration ratios, they found the atomization process within the plasma to be complete after 16 μs, and the concentration ratios of the elements in the plasma to be representative of the elemental ratios in the bulk solid.

Comparison of the relative LIF intensities of analytes measured in different matrices is based on two assumptions: (1) the samples are completely atomized in the portion of the plasma that is in the optical pathway of the probe beam, and (2) the plasma temperature is independent of the matrix. They found, however, that plasma temperatures did vary with the matrix, which influenced the degree of ionization of the analytes in various matrices. The Mn I/Mn II ratio (280.1 nm/257.6 nm) was the highest in the Al matrix (lowest plasma temperature), and lowest in the Cu plasma. While this ratio varied from one matrix to the next, it did not vary significantly with Mn concentration. As long as the analytes under investigation possessed ionization energies that were within one order of magnitude of each other and had similar lowest excited atomic state energies, the ratio of their ground-state populations would be, to a first approximation, independent of the plasma temperature. This condition was met by Mn, Cr, Si, and Mg, which were the analytes investigated. It was also concluded that the ratios of the ground-state atoms were independent of the amount of ablated material. This was important when the surface and/or the composition of the bulk of the matrix sampled varied, causing shot-to-shot fluctuations in the quantity of the vaporized sample.

Grant, Paul, and O'Neill[68] examined the emissions of laser plasmas form as a function of time for different samples. Using the 308-nm output of a XeCl excimer laser (focusing the 40 mJ, 28-ns pulses to a spot size of 0.9 mm^2), they determined the optimum delay time for the detection of Fe, Si, Mg, Ti, and Ca following the initial plasma-producing laser pulse. The samples were rotated between each

laser pulse, providing a fresh surface for each plasma formation. The temporal profile of the plasma emission was examined at several wavelengths and they found that the continuum, as measured at 389.61 nm for background only and at 389.56 nm for background plus Fe(I), was emitted within 10 ns of the arrival of the laser pulse and rose linearly to a maximum within 100 ns, then decayed in an exponential fashion, falling to zero after 2 μs. The atomic lines began to emerge above the continuum after 250 ns, with the Fe(I) 389.56 nm and Si(I) 390.55 nm lines appearing first in time and remaining strong throughout the lifetime of the plasma emission. The Mg(I) 518.36 nm, Ca(I) 431.86 nm, and Ti(I) 498.17 nm lines reached their maximum intensities at a later time. It was reported that the atomic lines for all these elements became better resolved at later times and, in general, linewidths narrowed and overlap interference decreased as the plasma cooled. The optimum detection time was found to be between 2 and 3 μs after the onset of the plasma formation. The variation in time of the maximum of the different components was not great enough to warrant changing the delay time for each one. One big advantage to using a delay time followed by a gated detection time was the large improvement in the signal-to-background ratios.

In a subsequent article, the same authors reported quantitative determinations of the elements in standard iron ore samples.[69] The resulting calibration curves for Ca, Si, Mg, Al, and Ti are shown in Figure 5. It was noted that lines for S and P were not observed with this technique, although some of the samples contained as much as 0.12% S and 0.72% P. The strongest lines of these two elements occur in the vacuum ultraviolet region and thus would not be detectable in air at atmospheric pressure. However, strong lines in the near ultraviolet and visible, 469.41 nm for S and 253.56 nm for P, were not detected.

Analysis of certified low alloyed steel samples by optical emission spectrometry (OES) and laser-induced fluorescence probing of laser-produced plumes was reported by Niemax and Sdorra.[70] The fundamental beam of a Nd:YAG laser was used to form the plasma on the sample surface. The sample was mounted inside a pressure chamber, allowing control of the buffer gas pressure. Emissions from the plasma were analyzed by an OMA system. Laser-induced fluorescence was accomplished with two dye lasers pumped by one excimer laser. Approximately 30 ng of material was ablated by a 10-mJ laser pulse focused to a 100-μm diameter spot. Initially, there was a dense sample plasma near the target and a buffer gas plasma above it. The buffer gas plasma served as an energy reservoir for the evaporation of ablated droplets and particles that penetrated into it. The sample then became completely atomized as the two plasmas mixed to form a single plasma. During this process, the buffer gas cooled as some of its energy was transferred into atomization of the target material. In the first few microseconds of plasma formation in argon the plasma temperature exceeded 20,000 K. From their LIF results for Mg, Niemax and Sdorra observed a strong ionic fluorescence at the onset of plasma formation, while atomic fluorescence was absent. At times later than 60 μs, the atomization process was complete and the ratio of Mg ions to Mg atoms slowly decreased. Results for certified steel samples from NIST containing Mg, B, Si, Mn, Cr, Pb, and Sn were reported. The results from the optical emission spectra were in good agreement with the LIF results as long as the concentration of analyte in the sample was homogeneous.

Stoffels and co-workers[71] conducted a time-resolved study of solid samples containing U. The metallic U sample was ablated by a Nd:YAG laser pulse (20 ns, 10 mJ, 1064 nm), at a repetition rate of 10 Hz. The resulting emissions were collected with a fiber optic and were detected either by a PMT/interference filter system or by an intensified diode array using a monochromator/OMA system. The fiber optic could be placed at three locations to examine three different regions of the plasma. They found that the temporal resolution of the emissions contained three distinct portions. The first region began almost simultaneously with the laser pulse and had a half-width of 50 ns when buffer gas pressure was below 1.5 torr. (Above this pressure, the three temporal regions merge.) This region, which was referred to as the *spike*, was attributed to unresolved line emission from the complex U spectrum, as well as contributions from continuum radiation from free-free and free-bound transitions. When the fiber optic was positioned to collect emissions from the plasma core, no lines from the buffer gas were observed. Therefore, it was concluded that during the spike core emission was from target particles.

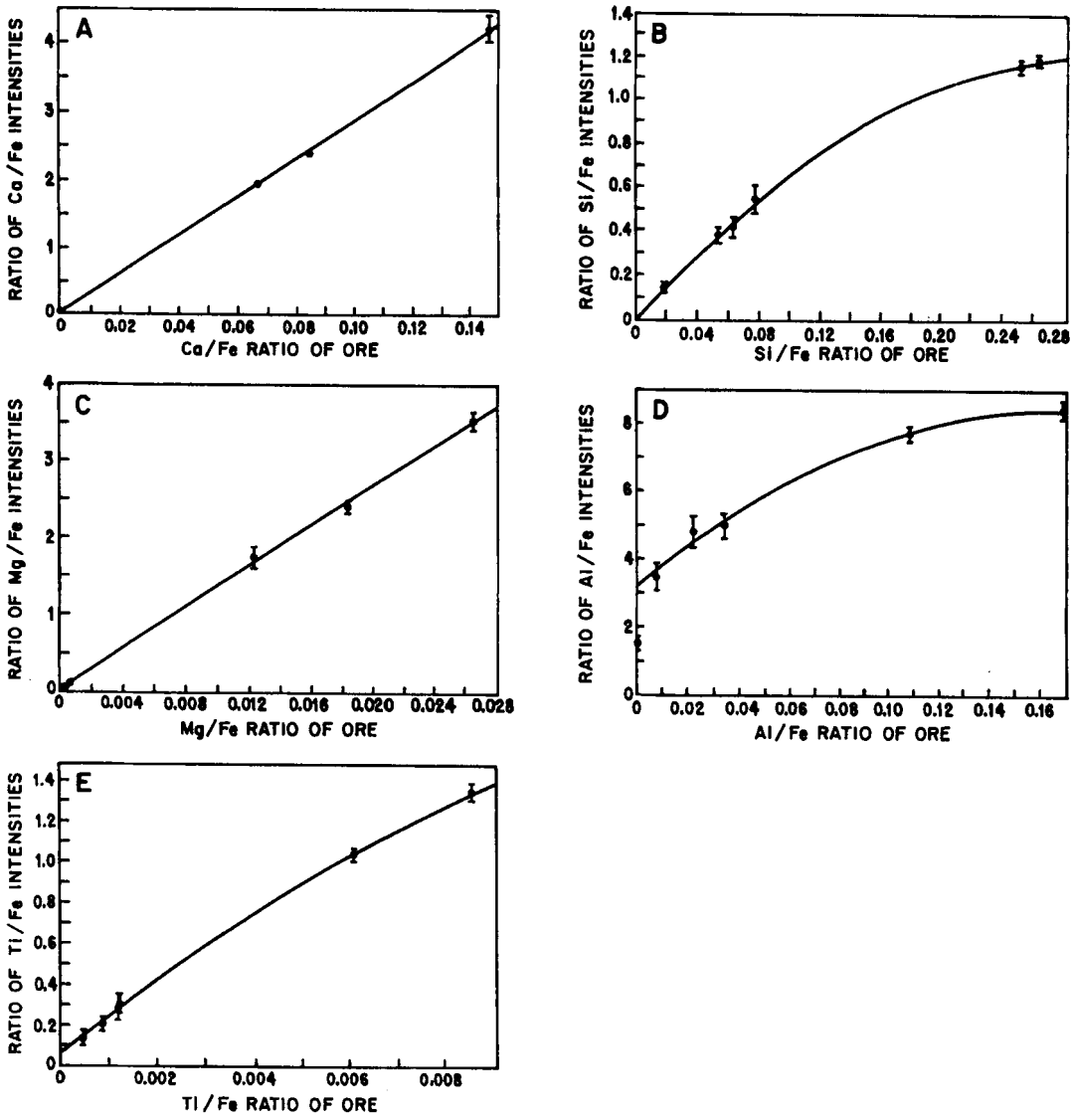

FIGURE 5. Calibration curves for (A) Ca, (B) Si, (C) Mg, (D) Al and (E) Ti in iron ore. The error bars indicate ± one standard deviation. (From Grant, K. G.; Paul, G. L.; O'Neill, J. *J. Appl. Spectrosc.* 1991, *45*, **703**. With permission.)

The second temporal region, 100 ns to about 5 μs, was referred to as the *first tail*. These were assigned to unresolved emission lines of U atoms and ions. The authors ruled out the possibility that these were line emissions superimposed on a continuum by observing that the line widths appeared small when compared with the line emissions of another element under comparable conditions. This region disappeared below 7.5 mtorr and above 1.5 torr buffer gas pressure, yet no emission from the buffer gas was observed. It was noted that the first tail maximum increased with pressure in air but decreased with pressure in argon.

The third region was called the *second tail*, appearing more than 5 μs after the laser pulse and at pressures between 0.075 and 0.75 torr. The intensity in this region was an order of magnitude lower than that of the first tail. In this temporal region, line structure was no longer observed, although the emissions were still due to the U. A UV band, appearing at 360 nm when air was the buffer gas, was attributed to uranium oxide. Above the upper limit, as well as below the lower limit, the temporal profile was a smooth curve. The second tail decayed much faster at lower pressures than at higher pressures.

The three regions, while pressure dependent, were distinct regardless of the nature of the buffer gas, suggesting that three different processes were occurring. However, the intensity ratios and time delays did vary greatly, both with pressure and with nature of buffer gas. While shot-to-shot plasma variations prevented quantitative comparisons, two trends were observed. Pressure increase resulted in an increase in the total radiation intensity, and the plasma decayed more rapidly in air than in argon.

In spectroscopic applications of LIP, the spatial characteristics of the plasmas, especially as they vary with the matrix, are important. Location of the plasma portion viewed by the detection system can be crucial to obtaining useful and consistent results. Lee et al.[72] reported space-resolved studies of Cu and Pb sample plumes that showed differences in appearance and volume. The 193-nm beam of an ArF excimer laser was used for ablation, and emission lines from the resulting plasma were monitored using a spectrometer photodiode array system. The detection system was mounted on a moving stage, allowing different regions of the plasma to be studied in increments of 0.05 mm.

The plasma formed on Cu had strong atomic and ionic emission signals as well as a strong background continuum near the surface, but a low background continuum in the outer sphere; the inner sphere of the plasma formed on the lead surface gave only atomic emissions. Boltzmann plot methods were used to determine plasma temperatures. Table 1 contains the spatial profile of the resulting temperatures as well as the correlation coefficients and linear equations of the fitted lines. The Cu plasma had higher temperatures than the Pb plasma, with the maximum value (17,200 K for Cu and 15,300 K for Pb) lying much closer to the target surface. This high temperature for the Cu plasma may have caused thermal ionization directly above the surface due to the higher thermal conductivity of copper compared to lead. As a result, the copper plasma contained a larger relative population of ions.

The lead surface gave rise to a larger plasma volume (extending 5 mm above the surface) than

TABLE 1
Correlations between Linear Fitting and Data in the Boltzman Plot

Metal	Axial dist. (mm)	Linear equation	Temp. (K)	Corr. constant
Copper[a]	0.1	$y = 16.670\text{-}1.0868\ e^{-4x}$	13,235	0.975
	0.2	$y = 17.017\text{-}9.0319\ e^{-5x}$	15,926	0.914
	0.3	$y = 17.323\text{-}8.4259\ e^{-5x}$	17,071	0.888
	0.4	$y = 17.503\text{-}9.0946\ e^{-5x}$	15,816	0.916
	0.5	$y = 17.073\text{-}9.0946\ e^{-5x}$	16,066	0.911
	0.6	$y = 16.811\text{-}9.2335\ e^{-5x}$	15,578	0.891
	0.8	$y = 15.939\text{-}8.3541\ e^{-5x}$	17,218	0.875
	1.0	$y = 15.741\text{-}8.6398\ e^{-5x}$	16,648	0.862
	1.4	$y = 15.485\text{-}9.2271\ e^{-5x}$	15,589	0.849
	1.8	$y = 14.916\text{-}8.9936\ e^{-5x}$	14,700	0.830
Lead[b]	0.8	$y = 11.908\text{-}1.0144\ e^{-4x}$	14,180	0.904
	1.0	$y = 12.635\text{-}1.0597\ e^{-4x}$	13,573	0.960
	1.2	$y = 12.635\text{-}1.0597\ e^{-4x}$	13,573	0.960
	1.6	$y = 12.634\text{-}1.0596\ e^{-4x}$	13,575	0.960
	1.8	$y = 14.436\text{-}9.4152\ e^{-5x}$	15,277	0.910
	2.0	$y = 14.892\text{-}9.8768\ e^{-5x}$	14,563	0.880
	2.4	$y = 16.020\text{-}9.8925\ e^{-5x}$	14,540	0.852
	3.0	$y = 15.527\text{-}1.0682\ e^{-4x}$	13,465	0.705
	3.6	$y = 14.136\text{-}1.2326\ e^{-4x}$	11,669	0.535

[a] Cu(I) lines used: 427.51, 465.11, 510.55, 515.32, 521.82 nm.
[b] Pb(I) lines used: 357.27, 363.96, 368.35, 373.99, 405.78 nm.

From Lee, Y. I., *et al., Appl. Spectrosc.*, 1992, *46*, **439**. With permission.

that of copper (extending only 2 mm above the surface). The relative intensities of the atomic lines for copper and lead as a function of axial distance are illustrated in Figure 6.

Considering the contents of the papers reviewed thus far, it is obvious that the relative densities of atoms and ions produced in an LIP vary with both the location inside the plasma and the time delay after the initial plasma formation. By far, the greatest obstacle to the use of LIP in analytical applications has been its low reproducibility. Systematic study of the temporal and spatial characteristics of the laser plume is necessary to control the factors creating fluctuations and to interpret the data obtained. Sdorra and Niemax[73] conducted a systematic examination of the plasma plume produced through irradiation of an 8-ns, 9-mJ, 1064-nm Nd:YAG laser beam onto a Cu sample containing a trace amount (298 μg/g) of Mg (8 ns, 9 mJ at 1064 nm). The sample was placed inside a chamber filled with argon as the buffer gas and the relative densities of Mg(I) and Mg(II) were measured by exciting the 285.21- and 280.27-nm transitions. An excimer-pumped dye laser beam excited a carefully controlled location of the laser plume at a programmed time delay. The resulting fluorescence was detected by a time-gated, intensified OMA system. The effect of changing the buffer gas pressure was also examined.

The magnesium ion-to-atom ratio was found to be extremely high when the plasma was probed at very short delay times. This ratio decreased very rapidly with time until, after delays greater than 60 μs, the rate of decrease in this ratio slowed down. This was the time delay region used to gate the dye laser probe beam, in conjunction with a 300-ns window that reduced the magnitude of the emission spectrum.

The spatial distribution of the Mg(I) and Mg(II) species within the plasma was examined in a vertical direction above the surface and lateral directions perpendicular to the laser beam. Data from one set of measurements, taken at a 1.5-mm height above the sample is presented in Figure 7. This figure shows that ionic species were more numerous than atomic species early in the plasma lifetime and were more strongly concentrated toward the center of the plasma. The atomic species population continued to increase until it reached a maximum, between 55 and 120 μs. At these later times, a larger portion of the atomic species was located near the plasma center.

Franzke, Klos, and Wokaun[74] used the unfocused (2 mm diameter) output of an excimer-pumped dye laser to irradiate a variety of inorganic solids with approximately 8-mJ pulses. Emissions were detected by a monochromator/CCD camera. Solids like $CaCO_3$, $BaCO_3$, halides, oxides, and crystalline

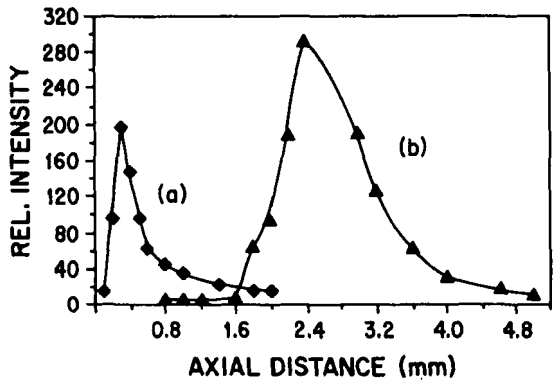

FIGURE 6. Spatial distribution of the plasma emission intensity of Cu(I) at 465.1 nm and Pb(I) at 405.78 nm. (a), copper; (b), lead. (From Lee, Y. I. et al. *Appl. Spectrosc.* 1992, *46*, **439**. With permission.)

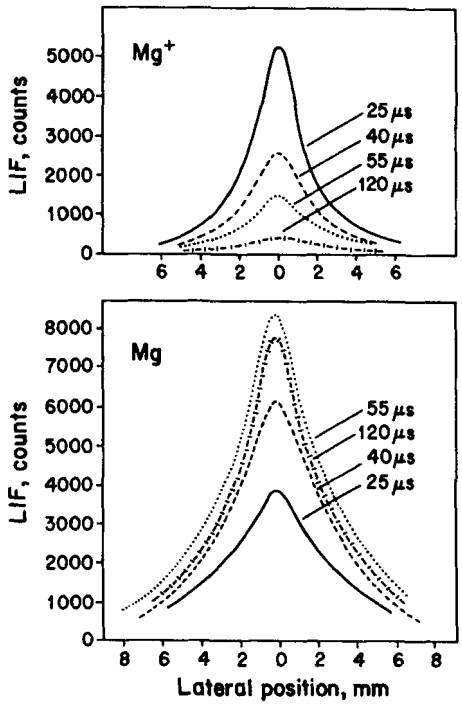

FIGURE 7. LIF of Mg(I) and Mg(II) lines measured at various delay times as a function of distance. (From Sdorra, W.; Niemax, K. *Spectrochim. Acta*, 1990, *45B*, **925**. With permission.)

sulfur, as well as reflecting metals such as copper, did not produce detectable emissions at this irradiance. Preliminary work on Cu surfaces with a focused laser beam, which increased the irradiance by a factor of 10^4, did create observable emissions. Other surfaces, composed of ZrO_2, $PbCrO_4$, K_2S, Sb_2S_3, and Mo_2S_3, gave observable atomic emission lines upon irradiation by the unfocused beam. $FeCuS_2$ gave detectable Fe(I) emissions, but no observed Cu or S emissions.

Three minerals, FeS_2, PbS, and ZnS were also investigated. With these targets, a single pulse created a visible spherical flash as well as an audible detonation. While pyrite (FeS_2) produced only lines belonging to Fe(I) transitions, zinc blende (ZnS) produced Zn(I), Fe(I), and Mn(I) lines. Iron and manganese are known contaminants of zinc blende. Weaker, but detectable characteristic emissions of calcium atomic and ionic lines as well as the strong lead atomic lines, were found in the PbS emission spectrum. The authors concluded that even strongly ionic compounds must dissociate into atoms rather than ions following this process of laser-induced desorption of the molecules. No emissions from any charge state of sulfur or oxygen were observed, although pure sulfur targets produced some emission lines that were thought to be due to neutral or charged sulfur clusters.

In the same paper, aqueous solutions were deposited and dried on solid targets. These targets were then subjected to laser plasmas. Initially, these solutions were deposited on inert surfaces such as glass or quartz. The subsequent irradiation by the laser pulse did not produce detectable emissions, a result that the authors attributed to insufficient sample material entering the plasma volume. When targets that were easily ablated (such as copper or brass) were used, three Pb(I) lines from a 100 mg/l $PbCl_2$ solution were detected. When a 10-mg/l solution was used, only the strongest line was detected. Further studies using 10-mg/l solutions of $HgCl_2$, $AgNO_3$, $FeCl_2$, and $CuCl_2$ did not produce detectable emissions under the same excitation conditions.

Spectrochemical analysis of milk powder by LIP was conducted by Kagawa and co-workers.[75] Varying ratios of milk powder to KBr were mixed and pressed to form pellets. These samples were mounted in a vacuum chamber that was then pumped down to 1 torr. The 10.6-μm output (3 J, 100 ns pulse) of a TEA CO_2 laser was attenuated to 300 mJ by an aperture and focused by a Ge lens to form a plasma on the sample surface. Calibration samples were made using $CaCO_3$ mixed with KBr. The resulting emissions were collected simultaneously by two monochromators at 422.6 nm [Ca(I) emission] and at 404.4 nm [K(I) emission]. These two lines provided an internal standard correction to compensate for the shot-to-shot fluctuation in the plasma emission.

The plasma formed in this low pressure system was quite large, with an approximate radius of 30 mm. The plasma dimensions decreased as the pressure increased. The calibration of the Ca(I)/K(I) intensity ratio was linear as a function of concentration (w/w). The detection limit of Ca in milk powder with their system was approximately 10 mg/l. They attributed the high LOD to the shot noise of the photomultiplier and suggested that using an OMA or a polychromator would improve this greatly.

Ottesen and co-workers[76] applied LIP techniques to the analysis of two different types of visible contaminants found on an inventory of electronic microcircuit boards. The problem faced was to determine the composition, to locate the source, and to evaluate the effect of the contaminant on the working components. Customary surface analysis techniques such as electron microscopy and Auger electron spectroscopy were not suitable due to the dielectric nature of the alumina substrate. It was desirable to keep the components in working condition, so analysis without destruction of the circuit was needed. Using LIP allowed for the vaporization of a minute amount of material from the contaminated area while at the same time exciting the plume, providing an emission spectrum that identified the elements present.

The first contaminant was a gray layer spread uniformly over the entire surface of several boards. It was found to contain Ni and Cr, which were not components of any of the microcircuit layers. Figure 8 shows the laser spark emission spectra of contaminated alumina substrate, clean substrate, and calculated emission spectrum for Cr(I). The peaks at either edge that are present only in the contaminated sample are due to Ni. The source of the contamination was traced to the racks used to hold the substrates during heating that had come from a different laboratory where chromic acid was used

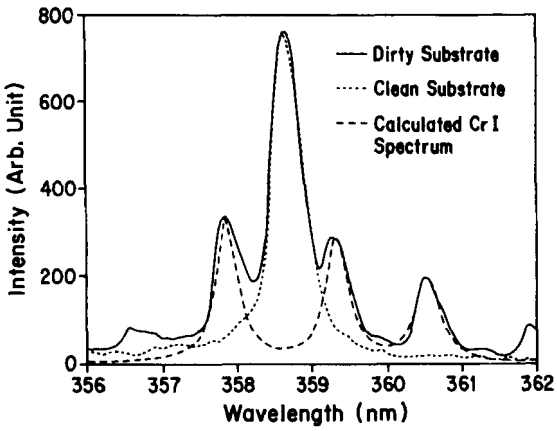

FIGURE 8. LIP spectra of contaminated alumina substrate (solid), clean alumina substrate (dash), and calculated Cr(I) emission spectrum (dot). (From Ottesen, D. K. *Appl. Spectrosc.* 1992, *46*, **594**. With permission.)

for cleaning. It was hypothesized that incomplete rinsing of previous items placed on the racks to dry had left traces of chromic acid that were subsequently vaporized during heating of the microcircuit boards and redeposited evenly on them as they cooled.

The second contaminant, which was a yellow stain, was found to contain Ca and Si. Analyzing the various layers of the microcircuit boards led to the conclusion that the stains were from the paste medium used to form the conductors. It was concluded that neither contaminant would interfere with the functioning of the microcircuit boards.

2. Liquids

Laser-induced plasmas may be used to spectroscopically probe the composition of liquid samples, either by focusing the laser beam to form a plasma in the bulk liquid or by focusing it at the surface, thereby vaporizing some of the liquid and observing the emissions from the plasma formed at the liquid/gas interface.

Laser plasmas formed in distilled and tapwater were recorded using streak photography by Docchio et al.[77,78] They found a significant lowering of the breakdown threshold in tapwater compared with distilled water. The plasma formed at the focal point and then expanded toward the laser. The emissions emanating from near the focal point did not last as long as the emissions from the upstream expansion region. In distilled water, the location of the initial plasma spark was reproducible, while the location of the initial spark in tapwater changed from shot to shot. As the intensity of the laser radiation increased, the plasma formed in tapwater consisted of a string of many small sparks contained within a main envelope. For reference purposes, studies were also conducted in polymethyl methacrylate, which exhibited an intense recombination luminescence.

The development of medical applications of lasers has motivated continuing work on characterizing the plasma formation mechanism in liquids. Results reported by Sacchi[79] include studies done in double-distilled water, 0.9% saline solution, tapwater, HPLC-grade water, and in fresh calf vitreous. This study considered mainly the effect of laser beam intensity and pulse duration on the breakdown thresholds in the various media.

With the goal of determining the U content in liquid streams at nuclear fuel facilities, Wachter and Cremers[80] selected LIP as the preferred method allowing for *in situ* monitoring. The determinations were to be carried out rapidly, and due to the nature of the analyte, sample handling needed to be minimal if not avoided completely.

Uranium solutions ranging from 0.1 to 100 g/l made through dilution with 4 *M* HNO_3 stock solution were used for calibration. The solutions were placed in sealed glass vials and oriented with the flat ends of the vial parallel both to the laser beam and to the detection system's optical pathway. Pulsing at a typical repetition rate of 9 Hz, the fundamental output of a Nd:YAG laser (~275 mJ/pulse) was focused to form a plasma at the surface of the solution. The plasma was formed partially in the liquid and partially in the gas above the liquid. The plasma light was detected with the use of a diode array rapid scanning spectrometer system.

Movement of the liquid surface due to splashing caused by the plasma shock wave propagation caused a fluctuation in shot-to-shot results. Precision improved when more than 200 laser spark spectra were averaged. Typically, 1200 sequential pulses were averaged and the net U signal was calculated as the peak height above the background. Application of this method of analysis to a flowing stream should be possible if there is sufficient information about the other components in the liquid, necessary for eliminating possible spectral interferences.

In order to develop a technique for detecting and determining the concentrations of monoatomic ions found in fluid inclusions in geological samples, LIP emission spectroscopy has been applied to solutions of cations.[81] A Nd:YAG laser beam was focused to form a plasma on the surface of a solution containing the analyte and the plasma emissions were detected with a multichannel spectrometer. Solutions of $CaCl_2$ and $MgCl_2$ were chosen for their initial studies because these two analytes could be simultaneously detected with their system.

After characterization of the solutions, synthetic inclusions were made from fractured quartz prisms, silica gel and the standard solutions that were loaded into gold capsules and heated, under 1.9×10^6 torr, at 920 K for 8 d. Analysis of the products showed synthetic fluid inclusions containing liquid and vapor phases at a 50% (v/v) ratio. The temporal behavior of the emissions was studied in order to optimize the analyte signal while minimizing both self-absorption and background emission. A typical emission spectrum of the synthetic fluid inclusions is shown in Figure 9. Ratios of the Ca /Mg line intensities had a linear relationship to the ratio of their concentrations.

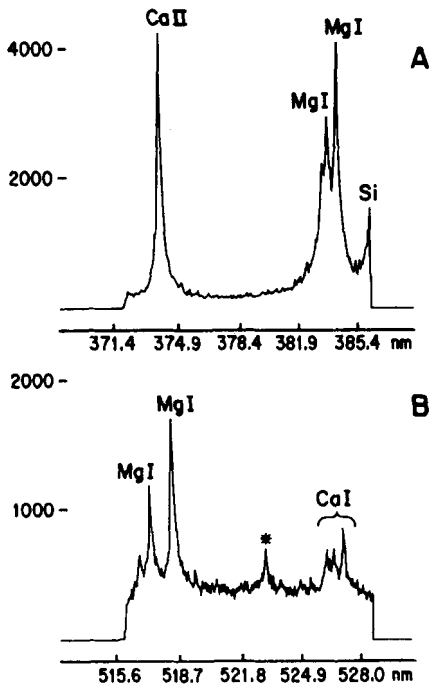

FIGURE 9. Typical emission spectrum of magnesium and calcium around 378 nm (A) and 522 nm (B) obtained on fluid inclusions. (*) Line not assigned. (From Boiron, M. C. et al. *Geochim. et Cosmochim. Acta.* 1991, *55,* **922**. With permission.

3. Gases

Determination of the composition of gas-phase samples presents an analytical challenge. Information about the composition of gaseous flows and production byproducts is important for industrial efficiency and safety. Obtaining a sample and then transporting it back to the laboratory for analysis is generally difficult. Furthermore, many determinations for pollution control purposes must be done at a distance. Because a laser beam can be focused through a window into virtually any container or flow system, as long as the emissions from the plasma can be detected, the use of LIP emission spectroscopy offers many possibilities.

Casini et al.[82] tested a laboratory version of a time-resolved laser-induced breakdown system that was designed to measure pollutant concentrations in air. The system used the fundamental output of a Nd:YAG laser to form a plasma in gas-phase samples, and then used a computer-interfaced stepping monochromator to detect the emissions from the plasma. To check the quantitative possibilities of the system, the ratio of oxygen to nitrogen in air was measured. This was accomplished by finding the ratio of the intensity of the N(II) (441.49 nm) to O(II) (444.7 nm) lines. By calibrating a pollutant's line intensity to a nearby line of nitrogen, which is always present in air with a relatively constant concentration, the amount of the pollutant can be determined.

Preliminary experiments conducted by Cheng, Fraser, and Eden,[83] applying LIP to samples of PH_3, AsH_3, and B_2H_6 in helium, gave promising results. A stainless steel chamber was designed to hold the sample for either a flowing or static fill of the analyte/helium mixtures. When no detectable difference in the results for the two methods was observed, static fill was used for these toxic gas studies. The second harmonic (532 nm) beam of a Nd:YAG laser was focused inside the sample chamber. Visible and UV radiation from the resulting plasma were collected perpendicular to the laser beam by a lens telescope/spectrometer combination that included two intensified diode arrays and an OMA detector.

Four phosphine mixtures at 3, 10, 50, and 180 μg/g in He were prepared. The 604.3-nm P(II) line and the 656.3-nm H(I) line were monitored. Above 20 to 30 μg/g PH_3 concentrations, the time-integrated 604.3-nm transition intensity was logarithmic in PH_3 concentration. Measurements below 10 μg/g were hampered by the background continuum. Thus, the minimum detectable concentration reported in this work was 3 μg/g PH_3.

The most reliable atomic transitions for the arsine studies were between 220 and 290 nm. Five As(I) lines were detectable in a 10-μg/g AsH_3/He sample. The detection limit was estimated to be 1 μg/g. In a similar fashion, studies of diborane dilutions in helium gave a detection limit of 1 μg/g when B(I) lines at 434.5 and 336.0 nm were used.

The authors suggest experimental design improvements, such as using a fiber optics bundle inside the vacuum chamber to detect more of the analyte emissions. They predicted that this modification, along with utilizing synchronous detection techniques, would lower the detection limit by as much as one order of magnitude.

B. Mixed Phase and Hyphenated Systems

Industrial systems are more often flow processes than batch processes. Solid samples and solid byproducts are frequently moved through the system by a carrier gas or by a flowing liquid. Occasionally, liquid flows are best sampled as aerosols, droplets aspirated into a gas stream. The challenge posed by these situations is to trigger plasma production and data collection only when a particle or droplet is present in the focal volume. As the threshold for plasma production in decreasing order is gas > liquids > solids, a laser beam whose power density is below the threshold for the carrier gas (or liquid), but above that for the particle or droplet, can generate a plasma when the species of interest enters the focal volume. The light from the resulting spark as plasma formation begins will trigger the data collection system.[84,85] Some systems use a stream of droplets synchronized to arrive in the focal volume with the laser pulse.[86,87] For this arrangement, no additional triggering of the data collection system is necessary. One system counted ultra-fine particles in ultra-pure water by detecting the acoustic shock wave produced by the plasma initiation.[88,89] Other hyphenated systems introduce the analyte into the plasma volume by methods such as nebulization of a solution followed by dehydration and then transported it into the plasma by the carrier gas flow.[90] In our laboratory, we have developed an instrumental arrangement that produces the plasma inside a graphite furnace. As the furnace is resistively heated, the previously dried sample vaporizes into the plasma volume.[91,92]

Ottesen and co-workers[85] developed a method of making simultaneous measurements of the size, velocity, and elemental composition of particles in a coal combustion system. LIP was used for the elemental analysis and it is that portion of their work that is discussed here. In a laboratory simulation of an industrial environment, coal samples were ground and then introduced into a stream of nitrogen gas. Downstream from the sample injection region, the particles passed through a region intersected by three laser beams just above a flat flame burner. Two of the lasers, a He-Ne and a Nd:YAG, were used for detecting a particle and then generating a laser spark on the particle. The resulting emissions were detected by an OMA system that was triggered when the light from the laser spark reached a silicon diode.

Calibration of the system was done using homogeneous particles composed of the ion exchange resin Amberlite, containing Ca and Mg. Figure 10 shows both the experimental and the calculated spectrum of a single ion-exchange resin particle loaded with 10 wt% Ca. The coal samples were ground up and introduced into the system for analysis. The bulk analysis of one of the three coal samples studied is shown on Table 2. Elements marked with an asterisk (*) were detected by LIP. In addition to these, trace amounts of the elements of Ba, Li, Mn, and Sr were detected.

Figure 11 shows the laser plasma spectrum of a single coal particle. By making some basic assumptions as to the plasma temperature, average density, average carbon content, approximate particle size based on measured particle diameter, and using the relative intensity of the Fe(II) and C(I) lines, the Fe content was computed to be about 520 fg.

Correlation of the LIP results for Si, Al, and Fe, relative to C, with the standard bulk chemical analysis of the same coal showed agreement within one order of magnitude. The authors attributed this difference to the lack of a temperature correction to the

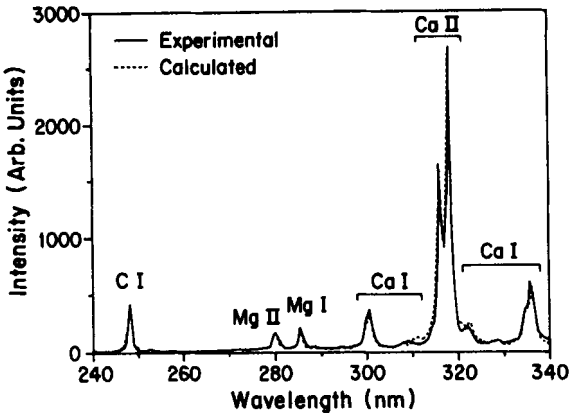

FIGURE 10. LIP spectrum of a single ion-exchange resin particle loaded with 10 wt% calcium. (From Ottesen, D. K.; Wang, J. C. F.; Radziemski, L. J. *Appl. Spectrosc.* 1989, *43*, **971**. With permission.)

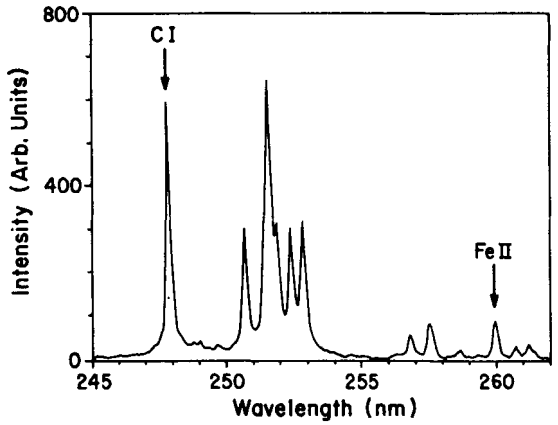

FIGURE 11. LIP spectrum showing 520 fg of iron detected in a single coal particle. (From Ottesen, D. K.; Wang, J. C. F.; Radziemski, L. J. *Appl. Spectrosc.* 1989, *43*, **973**. With permission.)

reference intensities in the laser plasma analysis. The major advantage of this system is being able to sample directly in the combustion environment, allowing for the possibility of real-time monitoring of this process on an industrial scale.

In a more recent work by Ottesen and co-workers,[84] emissions from nearly all of the inorganic elements present in coal in amounts greater than 100 μg/g were observed. Results that correlated well with standard bulk analysis were reported for Si, Al, Mg, and Ti. Difficulties due to self-absorption and occasional detector saturation for Fe and Ca were encountered.

TABLE 2
Bulk Analysis of Reference Coal

Pittsburgh high-volatile A bituminous (PSOC-1451 d) (63–75 μm size fraction)

Major element analysis		Minor element analysis	
Element	Element % of dry coal	Element	Element % of dry coal
C*	81.0	SiO_2*	1.9
H*	5.2	Al_2O_3*	0.95
O*	7.3	TiO_2*	0.063
N*	1.3	Fe_2O_3*	0.31
S	1.0	MgO*	0.03
		CaO*	0.06
Ash	3.7	Na_2O*	0.01
		K_2O*	0.07

* Elements also detected by laser spark spectroscopy.

From Ottesen, D. K.; Wang, J. C. F.; Radziemski, L. J., *Appl. Spectrosc.* 1989, *43*, **972**. With Permission.

Due to the difficulties encountered when quantification was based on absolute emission intensities, measurement of the emission from an element such as C was used to normalize each result. Sufficient results were obtained to measure matrix effects and develop a set of correction terms that improved the agreement with those obtained by bulk analysis methods.

The capability of collecting this real-time data *in situ* and also the direct comparison of the composition of individual particles, as determined by LIP, to elemental ash content analysis by scanning electron microscopy demonstrated the powerful possibilities of LIP emission spectroscopy as an analytical tool. Future plans include investigating different coals, a range of particle sizes, and the effect of combustion variables on particle composition.

Using a nebulization/desolvation system to produce dry aerosol samples and introduce them directly into the plasma volume, Essien et al.[90] studied the LIP emissions of Cd, Pb, and Zn. Solution samples were generated into wet aerosols with a standard stainless steel pneumatic nebulizer. The wet aerosol was then carried into a heated desolvation chamber, through a modified Friedrichs condenser, then through a Cu chamber and introduced into the plasma volume through a nozzle tip that was placed close to the focal point of the lens focusing the laser beam.

The calculation converting from solution concentrations to airborne concentrations was done by measuring the overall sample introduction efficiency

based on a standard flame atomic absorption analysis of a filter used to collect the dry aerosol generated by passing 10.0 ml of 500 μg/ml Pb solution through the nebulization/desolvation system. The 10-Hz, 100-mJ/pulse fundamental beam of a Nd:YAG laser was focused by a 3-cm focal length lens to form the plasma. The trigger to begin data collection was generated at the onset of plasma formation as sensed by a fast photodiode. Delay time was optimized to minimize background and ionic emissions while maximizing the signal from neutral species.

Calibration curves for Cd, Pb, and Zn showed linearity at low concentrations and either saturation or curvature at higher concentrations. The concentrations investigated ranged from 1 to 100 μg/g, with the detection limits computed to be 0.019, 0.21, and 0.24 μg/g for Cd, Pb, and Zn, respectively. Matrix effects for samples made from the chloride, nitrate, and acetate of Pb, and the nitrate and chloride of Cd were compared. The effect of the addition of sodium to the Pb emission signal was studied. The plasma temperature was determined by the two-line Boltzman method and it was found to be near 6500 K at 20 μs and decrease to ~5500 K at 35 μs. The detection limits for Cd and Zn were low enough for monitoring according to the American Conference of Governmental Industrial Hygienists limits.

Majidi and co-workers reported combining a graphite furnace sample introduction system with LIP atomization and excitation to study Cd, Co, Pb, Al, and Hg.[91,92] They used an OMA system to temporally observe the analyte emissions as the graphite furnace heated to vaporize and then atomize the analyte. The fundamental beam of a Nd:YAG laser was focused to form a plasma inside the furnace tube directly below the dosing hole. Emissions from the analyte were collected through the dosing hole, at a delay time that had been optimized previously. In a second configuration of this system, the second harmonic (532 nm) beam was used and the analyte emissions were collected from the end of the furnace, thus detecting all the emissions emanating from the tube. A UV transmitting filter was used to protect the detector. Minimum detectable amounts ranged from 0.5 pg for Al to 5 μg for Hg.

Archontaki and Crouch used LIBS in connection with an isolated droplet generator flow injection analysis sampling system.[86] The fundamental of a Nd:YAG laser was used for plasma formation with the detection/data processing system using a scanning spectrometer, photomultiplier tube, and a boxcar averager. After evaluating the effect of the sampling introduction variables on the analyte signal, they conducted a quantitative study of Li, Na, Mg, Ca, Mn, and Al. The reported detection limits were in the low microgram per liter range.

The chances of success of a new analytical method frequently hinge on sufficient understanding of the process involved. Alexander and co-workers[87] studied the process of plasma formation in water droplets using elastically scattered incident radiation (ESIR). They used the 248-nm beam of a KrF excimer laser focused to a spot size about 10^4 μm^2. Photographs shown in Figure 12 are the images of the water droplet as it was penetrated by the focused laser beam forming a plasma on the far side of the droplet. The droplet began to expel liquid from the dark side and a plasma formed on the front surface of the drop, followed by expulsion of liquid toward the laser. The droplet was 60 μm in diameter and the plasma-forming laser pulse has a duration of 17 to 22 ns. A second excimer laser was used to generate a beam perpendicular to that of the first laser, crossing at the plasma volume. This beam illuminated the droplet, allowing for the temporal imaging of the plasma formation process to be recorded. Two fiber optic probes, connected to a computer interfaced streak camera, were oriented to collect temporal information about the transmitted pulse and the incident pulse. A spectrograph was used to monitor the broad-band emission and thus follow the onset and decay of the plasma. The material in the plume on the dark side of the droplet had an estimated velocity of 1500 m/s during the first 50 ns, while that of the expelled matter on the side of the droplet toward the focused laser beam was approximately 200 m/s. It becomes most evident that the portion of the droplet/plasma volume viewed by an emission detection system is important to the correct interpretation of the resulting spectra.

Taking advantage of the sound waves produced by the shock wave that results from the formation of a LIP, Kitamori et al. used a photoacoustic detection device with a focused second harmonic (532 nm) of a Nd:YAG laser to detect the presence of ultrafine particles in a stream of water.[88,89] The laser was operated at 20 Hz and the energy of each pulse was

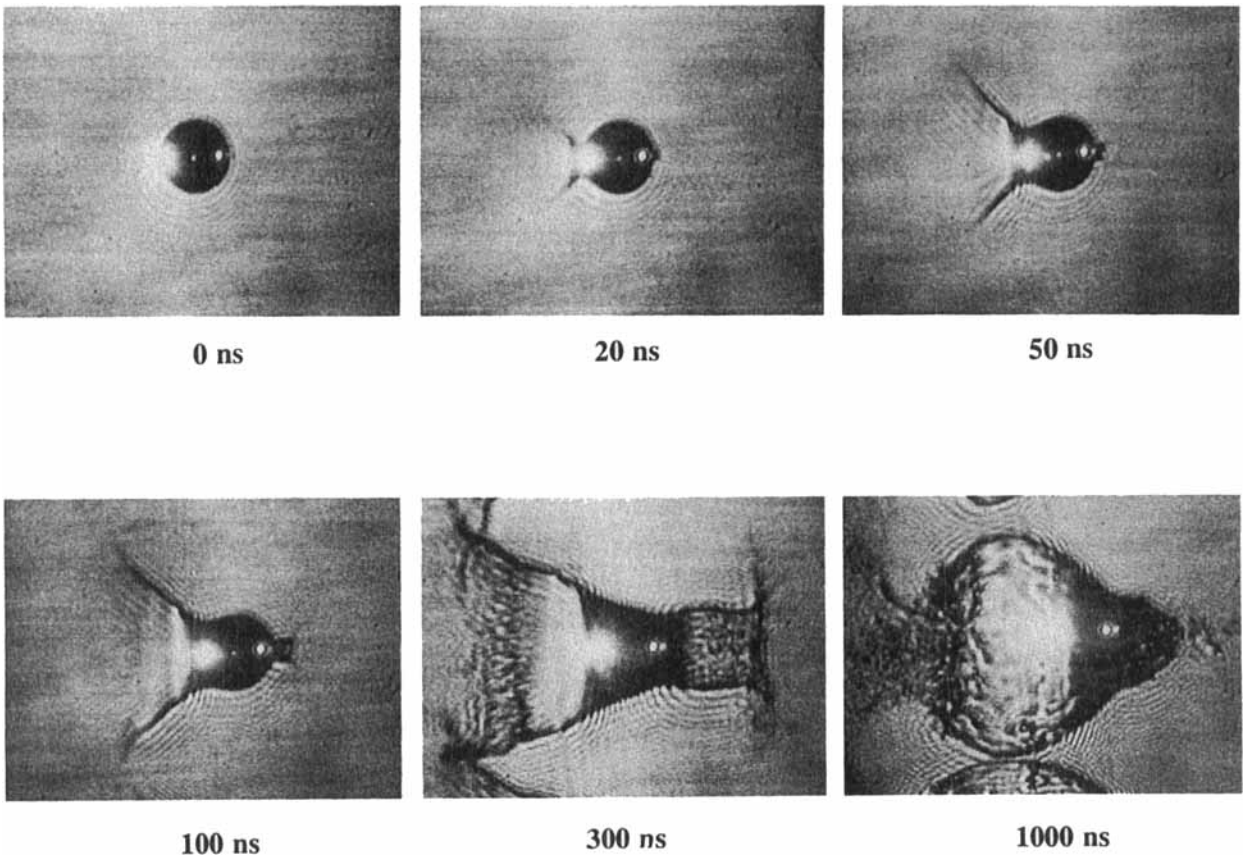

FIGURE 12. Typical images of 3-GW/cm2 KrF laser pulses incident upon 60-μm-diameter water droplets at 0, 20, 50, 100, 300, and 1000 ns after the arrival of the high-energy pulse. The high-energy pulse is propagating from right to left. The bright spots appearing on the illuminated and shadow surfaces of the droplet are produced by the 17-ns incident pulse saturating the vidicon. The lag in the vidicon makes these spots visible in later photographs. (Taken from Alexander, D. R. et al., *Optics Lett.*, 1989, *14*, **548**. Authors are with the Center for Electro-Optics, Room 248 WSEC, University of Nebraska, Lincoln, Nebraska 68588-0656. With permission.)

30 mJ with a duration of 10 ns. The irradiance of the laser beam was kept below the breakdown threshold of ultrapure water. Plasma formation occurred only when a 0.038-μm polystyrene ultrafine particle passed through the focal volume. They also found that only the particle, with a breakdown threshold smaller than the water or air bubbles, was broken down by the laser beam. The number densities of the particles in the ultrapure water ranged from 300 to 1200 ml^{-1}, corresponding to a weight concentration of 10^{-2} g/l. With 100-s long measurement periods giving 2000 laser pulses to each datum value, a linear relationship between number density and counts resulted. The particle size detectable by this method was one order of magnitude smaller than the conventionally used laser scattering method.

V. FUTURE TRENDS

LIPs are becoming popular in such diverse fields as microelectronic manufacturing, thin film deposition, laser processing, chemical synthesis, etc. Because the scope of this article was limited to the application of LIPs in spectrochemical analysis, the discussion of future trends is limited to that subject.

It is clear that laser plasma spectrochemical analysis is not the panacea that early researchers had hoped for. Yet LIP has been applied successfully to a variety of matrices as illustrated by the detection limits summarized in Table 3. However, some of the advantages afforded by these systems more than offset the limitations and ensures the longevity of LIP for analytical applications. For example, zero sample preparation has always been

TABLE 3
Representative Detection Limits

Element	LDM[a]	LOD[b]	Matrix	Ref.
Al	0.5 pg		Aqueous solution	91
As		0.5	Air	64
AsH_3		1	In helium	83
B_2H_6		1	In helium	83
Be		0.6 ng/g	Air	64
Ca		200	Fluid inclusions	81
Cd		0.018	Dry aerosols	90
Cd	50 pg		5% nitric acid	92
Cl		8	Air	93
Co	5 pg		5% nitric acid	92
F		38	Air	93
Hg		0.5	Air	64
Mg		25	Fluid inclusions	81
Na		6 ng/g	Air	64
P		1.2	Air	64
Pb		0.20	Dry aerosols	90
Pb	5 ng		Aqueous solution	91
PH_3		3	In helium	83
U		0.1 mg/g	0.4 % nitric acid	80
Zn		0.23	Dry aerosols	90

[a] Lowest detectable mass,
[b] Limit of detection, in µg/g except where noted.

a goal of analytical chemists and laser plasmas come closest to fulfilling the requirements for this task.

Because laser plasmas can be generated in any media, they should be regarded as a universal sampling, atomization, excitation, and ionization source. Each process could be individually tailored to some extent to match a specific application. If hyphenation with atomic absorption or inductively coupled plasma is needed, then the sampling and atomization process could be adjusted through beam geometry and power densities.[91] If ionization for mass spectrometric applications is desired, the wavelength and power density parameters could be optimized.[16] Hyphenation with other analytical instrumentation is another area in which laser plasmas will have a significant impact.

It is the authors' opinion that the next and the most promising arena for LIP is the application for remote sensing. As far as elemental analysis is concerned, no other remote probe can provide similar information to LIPs. Furthermore, it has already been demonstrated that laser plasmas can be utilized successfully for remote elemental analysis.[66] Atmospheric pollution monitoring, nonintrusive analysis of hazardous material, and fiber optic-based *in situ* analysis are only few of the applications for which LIP can provide unmatched performance.

REFERENCES

1. Mullen, R. A.; Matossian, J. N. *Opt. Lett., Quenching optical breakdown with an applied electric field*, 1990. *15*, **601**.
2. Briand, J.; Kieffer, J. C.; Gomes, A.; Arnas, C.; Dinguirard, J. P.; Quemener, Y.; Berge, L.; El, T. M.; Armengaud, M. *Phys. Fluids, Measurements of magnetic fields using the Zeeman effect in laser-produced plasmas*, 1987. *30*, **2893**.
3. Eliezer, S.; Arad, B.; Gazit, Y.; Kishenevsky, M.; Loeb, A.; Ludmirsky, A.; Yarkoni, E.; Zigler, A. *Laser Interact. Relat. Plasma Phenom., The use of magnetic fields in laser-produced plasmas for building a free electron laser*. 1988, *8*, **43**.
4. Mason, K. J.; Goldberg, J. M. *Anal. Chem., Observation of laser-induced anisotropy in ion acoustic waves in a plasma*. 1987, *59*, **1250**.
5. Mostovych, A. N.; Ripin, B. H.; Stamper, J. A. *Phys. Rev. Lett., Laser-produced plasma jets: collimation and instability in strong transverse magnetic fields* 1989, *62*, **2837**.

6. Preppernau, B. L.; Dolson, D. A.; Gottscho, R. A.; Miller, T. A. *Plasma Chem. Plasma Process., Temporally resolved laser diagnostic measurements of atomic hydrogen concentrations in RF plasma discharges.* 1988, *9*, **155**.
7. West, W. P.; Thomas, D. M.; deGrassie, J. S.; Zheng, S. B. *Phys. Rev. Lett., Spectroscopic diagnostics of plasma-chemical-vapor deposition from silane and germane.* 1987, *58*, **2758**.
8. Biswas, A.; Latifi, H.; Radziemski, L. J.; Armstrong, R. L. *Appl. Opt., Irradiance and laser wavelength dependence of plasma spectra from single levitated aerosol droplets.* 1988, *27*, **2386**.
9. Wood, O. R. I.; Silfvast, W. T.; Tom, H. W. K.; Knox, W. H.; Fork, R. L.; Brito, C. C. H.; Downer, M. C.; Maloney, P. J. *Appl. Phys. Lett., Effect of laser pulse duration on short wavelength emission from femtosecond and picosecond laser-produced tantalum plasmas.* 1988, *53*, **654**.
10. Weber, C.; Becker, U.; Renner, R.; Klingshirn, C. *Appl. Phys. B, Photophys. Laser Chem., Laser ionization mass spectrometry of* $YBa_2Cu_3O_{(7-x)}$ *superconductors.* 1988, *B45*, **113**.
11. Buchmann, L. M.; Heinrich, F.; Hoffmann, P.; Janes, J. *J. Appl. Phys., The CO2 laser-a new ultrasound source.* 1990, *67*, **3635**.
12. Jochum, K. P.; Matus, L.; Seufert, H. M. *Fresenius' Z. Anal. Chem., Trace element determination by laser plasma mass spectrometry.* 1988, *331*, **136**.
13. Martin, W. B.; Silly, L.; Murphy, C. M.; Raley, T. J. J.; Cotter, R. J.; Bean, M. F. *Int. J. Mass Spectrom. Ion Processes, Fragmentation of carbohydrates in laser desorption, plasma desorption and fast atom bombardment mass spectrometry.* 1989, *92*, **243**.
14. Vertes, A.; De, W. M.; Juhasz, P.; Gijbels, R. *Anal. Chem., Threshold conditions of plasma ignition in laser ionization mass spectrometry of solids.* 1989, *61*, **1029**.
15. Hogan, J. D.; Beu, S. C.; Ladue, D. A.; Majidi, V. *Anal. Chem., Probe-mounted fiber optics assembly for laser desorption/ionization Fourier transform mass spectrometry.* 1991, *63*, **1452**.
16. Owens, M. D.; Majidi, V. *J. Trace Microprobe Tech., Laser plasma desorption/ionization mass spectrometry for the analysis of solids* 1992, in press.
17. Jovicevic, S.; Konjevic, N.; Chapliev, N. I.; Konov, V. I.; Pimenov, S. M. *Appl. Phys. A, Solids Surf., CO_2 laser-induced plasma formation on a copper surface covered by dielectric particles.* 1989, *A48*, **283**.
18. Chylek, P.; Jarzembski, M. A.; Srivastava, V.; Pinnick, R. G.; Pendleton, J. D.; Cruncleton, J. P. *Appl. Opt., Effect of spherical particles on laser-induced breakdown of gases.* 1987, *26*, **760**.
19. Armstrong, R. L.; Zardecki, A. *Appl. Opt., Propagation of high energy laser beams through metallic aerosols.* 1990, *29*, **1786**.
20. Carls, J. C.; Brock, J. R. *Opt. Lett., Space-time resolved diagnostics of radio frequency glow discharge kinetics.* 1988, *13*, **273**.
21. Chitanvis, S. M. *J. Appl. Phys., A hydrodynamic model of plasma initiation off irradiated metallic aerosols in vacuum: the diffusive regime.* 1989, *65*, **1838**.
22. Lushnikov, A. A.; Maksimenko, V. V.; Pakhomov, A. V. *J. Aerosol Sci, Fractal aggregates from laser plasma.* 1989, *20*, **865**.
23. Mertens, P.; Bogen, P. *Appl. Phys. A, Time-resolved spectroscopy of plasmas initiated on single, levitated aerosol droplets.* 1987, *A43*, **197**.
24. Steinman, D.; Caldwell, V.; Husband, D.; Ruppe, J.; Welch, S. *J. Vac. Sci. Technol. A, Vac. Surf. Films, Temporally and spatially resolved spectroscopy of laser-induced plasma from a droplet.* 1988, *6*, **2**.
25. Zheng, J. B.; Hsieh, W. F.; Chen, S. C.; Chang, R. K. *Opt. Lett., Temporally and spatially resolved spectroscopy of laser-induced plasma from a droplet.* 1988, *13*, **559**.
26. Eickmans, J. H.; Hsieh, W. F.; Chang, R. K. *Opt. Lett., Laser-induced explosion of water droplets: spatially resolved spectra.* 1987, *12*, **22**.
27. Harith, M. A.; Palleschi, V.; Salvetti, A.; Singh, D. P.; Tropiano, G.; Vaselli, M. *Opt. Commun., Experimental studies on shock wave propagation in laser produced plasmas using double wavelength holography.* 1989, *71*, **76**.
28. Harith, M. A.; Palleschi, V.; Salvetti, A.; Singh, D. P.; Tropiano, G.; Vaselli, M. *Opt. Commun., Experimental studies on shock wave propagation in laser produced plasmas using double wavelength holography.* 1989, *71*, **1**.
29. Cappelli, M. A.; Paul, P. H.; Hanson, R. K. *Laser Part. Beams, Laser-induced fluorescence imaging of laser-ablated barium.* 1990, *8*, **1**.
30. Khan, T. P. *Ind. J. Pure Appl. Phys., Power meter for optical efficiency measurements of laser-induced plasmas.* 1987, *25*, **355**.
31. Takiyama, K.; Kamiura, Y.; Fujita, T.; Oda, T.; Sakai, H.; Kawasaki, K. *Jpn. J. Appl. Phys., Production and confinement of thermal energy multiply charged ions from laser-induced plasma for charge transfer studies.* 1987, *26*, **1945**.
32. Cappelli, M. A.; Measures, R. M. *Appl. Opt., Electron density radial profiles derived from Stark broadening in a sodium plasma produced by laser resonance saturation.* 1987, *26*, **1058**.
33. Yamada, K.; Tetsuka, T.; Deguchi, Y. *J. Appl. Phys., Nonequilibrium description of the intense resonant laser excitation of a semiconductor.* 1990, *67*, **6734**.
34. Grant, K. G.; Paul, G. L. *Appl. Spectrosc., Electron temperature and density profiles of excimer laser-induced plasmas.* 1990, *44*, **1349**.
35. Goldstein, W. H.; Walling, R. S.; Bailey, J.; Chen, M. H.; Fortner, R.; Klapisch, M.; Phillips, T.; Stewart, R. E. *Phys. Rev. Lett., Independent determinations of temperature and ionization balance in a laser-produced plasma by use of L-shell X-ray spectra.* 1987, *58*, **2300**.
36. Vertes, A.; Juhasz, P.; De, W. M.; Gijbels, R. *Int. J. Mass Spectrom. Ion Processes, Hydrodynamic modeling of laser plasma ionization processes.* 1989, *94*, **63**.

37. Vertes, A.; Juhasz, P.; Balazs, L.; Gijbels, R. *Microbeam Anal., Target heating, plasma formation, and expansion processes during laser ionization.* 1989, *24*, **273**.
38. Marjoribanks, R. S. Thesis, Time-Resolved Spectroscopy of Nonequilibrium Ionization in Laser-Produced Plasmas. University of Rochester, Rochester, NY. 1988.
39. Coche, M.; Berthoud, T.; Mauchien, P.; Camus, P. *Appl. Spectrosc., Laser-enhanced ionization detection in a laser-produced plasma at atmospheric pressure: theoretical and experimental considerations.* 1989, *43*, **646**.
40. Apruzese, J. P.; Burkhalter, P. G.; Rogerson, J. E.; Davis, J.; Seely, J. F.; Brown, C. M.; Newman, D. A.; Clark, R. W.; Knauer, J. P.; Bradley, D. K. *Phys. Rev. A: Gen. Phys., Enhanced excitation and ionization of neonlike silver in laser-produced plasmas simultaneously irradiated by two wavelengths.* 1989, *39*, **5697**.
41. Ratliff, J.; Majidi, V. *Anal. Chem., Simultaneous meassurement of the atomic and molecular absorption of Al, copper, and Pb nitrate in an electrothermal atomizer*, 1992, *64*, in press.
42. Majidi, V.; Ratliff, J.; Owens, M. *Appl. Spectrosc., Investigation of transient molecular absorption in a graphite furnace by laser-induced plasmas.* 1991, *45*, **473**.
43. Dietze, H. J.; Becker, S. *Int. J. Mass Spectrom. Ion Process., Properties of a laser-plasma X-ray source for X-ray lithography.* 1988, *82*, **1**.
44. Moustaizis, S. D.; Tatarakis, M. K.; Doukas, A.; Charalambidis, D.; Garkas, G. Y.; Horvath, Z.; Toth, C. S. *Bull. Acad. Sci. USSR Phys. Ser., Enhancement of the X-ray emission of laser-induced plasma in the presence of a high static electric field.* 1989, *1140*, **436**.
45. Selwyn, G. S.; Singh, J.; Bennett, R. S. *J. Vac. Sci. Technol. A, Vac. Surf. Films, Investigations on laser plasma soft X-ray sources generated with low energy laser systems.* 1989, *7*, **2758**.
46. Wellegehausen, B.; Hube, M. *Laser Optoelektron., Laser-induced plasmas as X-ray pump source for short-wavelength lasers.* 1988, *20*, **58**.
47. Li, Y.; Xu, Z.; Chen, S.; Wang, X.; Jiang, Z.; Feng, X. *Phys. Rev. A, Space-resolved investigation of soft-X-ray emission characteristics of a laser plasma in a half-cylindrical shell target.* 1990, *41*, **4528**.
48. Toubhans, I.; Fabbro, R.; Gauthier, J. C.; Chaker, M.; Pepin, H. *Proc. Spie Int. Soc. Opt. Eng., X-ray conversion efficiency in laser-produced plasmas. Application to X-ray lithography.* 1989, *1140*, **358**.
49. Wellegehausen, B.; Hube, M.; Jin, F. *Appl. Phys. B, Investigations of laser plasma soft X-ray sources generated with low energy laser systems.* 1989, *B49*, **173**.
50. Kuehlke, D.; Herpers, U.; Von, d. L. D. *Appl. Phys. Lett., Soft X-ray emission from subpicosecond laser-produced plasmas.* 1987, *50*, **1787**.
51. O'Neill, F.; Davis, G. M.; Gower, M. C.; Turcu, I. C. E.; Lawless, M.; Williams, M. *Proc. Spie Int. Soc. Opt. Eng., Plasma X-ray sources for lithography generated by a 0.5 J krypton fluoride (KrF) laser.* 1988, *831*, **230**.
52. Kuehlke, D.; Herpers, U.; Von, d. L. D. *Proc. Spie Int. Soc. Opt. Eng., X-ray flashes from plasmas generated by subpicosecond laser pulses.* 1988, *831*, **91**.
53. Scott, R. H.; Strasheim, A. *Spectrochim. Acta, Laser-induced plasmas for analytical spectroscopy.* 1970, *25B*, **311**.
54. Loree, T. R.; Radziemski, L. J.; Cremers, D. A. *Electro-Optical System Design, AES by LIBS may help you.* 1982, *14*, **35**.
55. Adrain, R. S.; Watson, J. *J. Phys. D: Appl. Phys., Laser microspectral analysis: a review of principles and applications.* 1984, *17*, **1915**.
56. Blades, M. W.; Banks, P.; Gill, C.; Huang, D.; Le Blanc, C.; Liang, D. *IEEE Trans. Plasma Science, Application of weakly ionized plasmas for material sampling and analysis.* 1991, *19*, **1090**.
57. Thiem, T. L.; Lee, Y.-I.; Sneddon, J. *Michrochem. J., Lasers in atomic spectroscopy: selected applications.* 1992, *45*, **1**.
58. Chang, R. K.; Eickmans, J. H.; Wen, F. H.; Wood, C. F.; Jian, Z. Z.; Jia, B. Z. *Appl. Opt., Effective photoconductivity and plasma depth in optically quasi-CW controlled microwave switching devices.* 1988, *27*, **2377**.
59. Bobin, J. L. *Phys. Scr., In-situ particulate contamination studies in process plasmas.* 1990, *T30*, **77**.
60. Raizer, Y. P. *Laser-Induced Discharge Phenomena;* Consultants Bureau: New York, 1977.
61. *Laser-Induced Plasmas and Applications*; L. J. Radziemski, D.A. Cremers, Eds.; Marcel Dekker: New York, 1989.
62. Maker, P. D.; Terhune, R. W.; Savage, C. M., in *Third Int. Congress*; Columbia University Press: Paris, 1963; pp. **1559**.
63. Bettis, J. R. *SPIE-Int. Opt. Mat., Correlation between the laser-induced breakdown threshold in solids, liquids, and gases.* 1990, *1441*, **521**.
64. Radziemski, L. J.; Loree, T. R.; Cremers, D. A.; Hoffman, N. M. *Anal. Chem., Time-resolved laser-induced breakdown spectrometry of aerosols.* 1983, *55*, **1246**.
65. Boland, B. C.; Irons, F. E.; McWhirter, R. W. P. *J. Phys. B. (Proc. Phys. Soc.), A spectroscopic study of the plasma generated by a laser from polyethylene.* 1968, *1*, **1180**.
66. Cremers, D. A. *Appl. Spectrosc., The analysis of metals at a distance using laser-induced breakdown spectroscopy.* 1987, *41*, **572**.
67. Quentmeier, A.; Sdorra, W.; Niemax, K. *Spectrochim. Acta, Internal standardization in laser-induced fluorescence spectrometry of microplasmas produced by laser ablation of solid samples.* 1990, *45B*, **537**.
68. Grant, K. J.; Paul, G. L.; O'Neill, J. A. *Appl. Spectrosc., Time resolved laser-induced breakdown spectroscopy of iron ore.* 1990, *44*, **1711**.
69. Grant, K. J.; Paul, G. L.; O'Neill, J. *Appl. Spectrosc., Quantitative elemental analysis of iron ore by laser-induced breakdown spectroscopy.* 1991, *45*, **701**.
70. Niemax, K.; Sdorra, W. *Appl. Opt., Optical emission spectrometry and laser-induced fluorescence of laser produced sample plumes*, 1990, *29*, **5000**.

71. Stoffels, E.; Van de Weijer, P.; Van der Mullen, J. *Spectrochim. Acta, Time-resolved emission from laser-ablated uranium.* 1991, *46B*, **1459**.
72. Lee, Y. I.; Sawan, S. P.; Thiem, T. L.; Teng, Y. Y.; Sneddon, J. *Appl. Spectrosc., Interaction of a laser beam with metals. Part II: Space-resolved studies of laser-ablated plasma emission.* 1992, *46*, **436**.
73. Sdorra, W.; Niemax, K. *Spectrochim. Acta, Temporal and spatial distribution of analyte atoms and ions in microplasmas produced by laser ablation of solid samples.* 1990, *45B*, **917**.
74. Franzke, D.; Klow, H.; Wokaun, A. *Appl. Spectrosc., Element identification on the surface of inorganic solids by excimer laser-induced emission spectroscopy.* 1992, *46*, **587**.
75. Kagawa, K.; Deguchi, Y.; Ogata, A.; Kurniawan, H.; Ikeda, N.; Takagi, Y. *Jpn. J. Appl. Phys., Emission spectrochemical analysis of food material using TEA CO_2 laser-induced shock wave plasma.* 1991, *30*, **L 1889**.
76. Ottesen, D. K. *Appl. Spectrosc., Detection of contaminants on electronic microcircuit substrates by laser spark emission spectroscopy.* 1992, *46*, **593**.
77. Docchio, F.; Regondi, P.; Capon, M. R. C.; Mellerio, J. *Applied Optics, Study of the temporal and spatial dynamics of plasmas induced in liquids by nanosecond Nd:YAG laser pulses. 1: Analysis of the plasma starting times.* 1988, *27*, **3661**.
78. Docchio, F.; Regondi, P.; Capon, M. R. C.; Mellerio, J. *Appl. Opt., Study of the temporal and spatial dynamics of plasmas induced in liquids by nanosecond neodymium-doped yttrium Al garnet laser pulses. 2: Plasma luminescence and shielding.* 1988, *27*, **3669**.
79. Sacchi, C. A. *J. Opt. Soc. Am. B, Laser-induced electric breakdown in water.* 1991, *8*, **337**.
80. Wachter, J. R.; Cremers, D. A. *Appl. Spectrosc., Determination of uranium in solution using laser-induced breakdown spectroscopy.* 1987, *41*, **1042**.
81. Boiron, M. C.; Dubessy, J.; Andre, N.; Briand, A.; Lacour, J. L.; Mauchien, P.; Mermet, J. M. *Geochimica et Cosmochimica Acta, Analysis of mono-atomic ions in fluid inclusions by laser-produced plasma emission spectroscopy.* 1991, *55*, **917**.
82. Casini, M.; Harith, M. A.; Palleschi, V.; Salvetti, A.; Singh, D. P.; Vaselli, M. *Laser and Particle Beams, Time-resolved LIBS experiment for quantitative determination of pollutant concentration in air.* 1991, *9*, **633**.
83. Cheng, E. A. P.; Fraser, R. D.; Eden, J. G. *Appl. Spectrosc., Detection of trace concentrations of column III and V hydrides by laser-induced breakdown spectroscopy.* 1991, *45*, **949**.
84. Ottesen, D. K.; Baxter, L. L.; Radziemski, L. J.; Burrows, J. F. *Energy & Fuels., Laser spark emission spectroscopy for in situ, real-time monitoring of pulverized coal particle composition.* 1991, *5*, **304**.
85. Ottesen, D. K.; Wang, J. C. F.; Radziemski, L. J. *Appl. Spectrosc., Real-time laser spark spectroscopy of particulates in combustion environments.* 1989, *43*, **967**.
86. Archontaki, H. A.; Crouch, S. R. *Appl. Spectrosc., Evaluation of an isolated droplet sample introduction system for laser-induced breakdown spectroscopy.* 1988, *42*, **741**.
87. Alexander, D. R.; Schaub, S. A.; Zhang, J.; Poulain, D. E.; Barton, J. P. *Opt. Lett., Scattering of incident KrF laser radiation resulting from the laser-induced breakdown of H_2O droplets.* 1989, *14*, **548**.
88. Kitamori, T.; Yokose, K.; Suzuki, K.; Sawada, T.; Gohshi, Y. *Jpn. J. Appl. Phys., Laser breakdown acoustic effect of ultrafine particle in liquids and its application to particle counting.* 1988, *27*, **L983**.
89. Kitamori, T.; Yokose, K.; Sakagami, M.; Sawada, T. *Jpn. J. Appl. Phys., Detection and counting of ultrafine particles in ultrapure water using laser-breakdown acoustic method.* 1989, *28*, **1195**.
90. Essien, M.; Radziemski, L. J.; Sneddon, J. *J. Anal. Atom. Spectrom., Detection of Cd, Pb and zinc in aerosols by laser-induced breakdown spectrometry.* 1988, *3*, **985**.
91. Joseph, M. R.; Majidi, V. *J. Trace Microprobe Tech., Laser-induced plasma atomic emission spectrometry of trace metals using an electrothermal atomizer.* 1992, in press.
92. Majidi, V.; Rae, J. T.; Ratliff, J. *Anal. Chem., Determination of trace metals using an electrothermal atomizer by laser-induced plasma atomic emission spectrometry.* 1991, *63*, **1600**.
93. Cremers, D. A.; Radziemski, L. J. *Anal. Chem., Detection of chlorine and fluorine in air by laser-induced breakdown spectrometry.* 1983, *55*, **1252**.